THE ASTROPHYSICAL JOURNAL, 430:850–857, 1994 August 1

AN ASTEROSEISMOLOGICAL DETERMINATION OF THE STRUCTURE OF THE DBV WHITE DWARF GD 358

P. A. BRADLEY[1] AND D. E. WINGET
McDonald Observatory and Department of Astronomy, University of Texas at Austin, Austin, TX 78712-1083
Received 1993 September 16; accepted 1994 January 28

ABSTRACT

We determine the structure of the pulsating DB white dwarf GD 358 through the technique of asteroseismology—where we compare our theoretical period distributions with the observational data. The observed periods are based on over 150 hours of nearly continuous high-speed photometric data obtained with the Whole Earth Telescope.

We find that GD 358 has a mass of $0.61 \pm 0.03\ M_{\odot}$ with a helium layer mass of $\log M_{\rm He}/M_{*} = -5.70^{+0.18}_{-0.30}$. Our results also constrain the structure of the helium/carbon transition zone and may have important consequences for our theoretical understanding of mixing and diffusion in white-dwarf stars.

Our best-fit models have a luminosity of $\log L/L_{\odot} = -1.30^{+0.09}_{-0.12}$; we use this to derive a distance of 42 ± 3 pc, consistent with the parallax value. This distance determination is completely independent of the parallax determination, and our errors are dominated by the uncertainty in effective temperature. In the future, accurate distances to white dwarfs derived from asteroseismology will offer us the opportunity to probe properties of the interstellar medium as a function of distance and allow us to use white dwarfs as tracers of the dynamics of the local Galactic disk.

Subject headings: stars: fundamental parameters — stars: individual (GD 358) — stars: oscillations — white dwarfs

1. INTRODUCTION

Asteroseismology gives us the opportunity to peer beneath the photosphere of stars with a clarity dependent on the number of modes available. With it, we have the potential to determine the stellar mass, compositional structure, transition zone profiles, rotation period, magnetic field strength, effective temperature, and luminosity of pulsating white dwarfs. White dwarfs have several major advantages for asteroseismology. First, they have many modes excited at once, giving us the potential for an exceptionally penetrating view of their interiors. Also, there are four distinct classes of degenerate pulsators spanning five orders of magnitude in luminosity, so we can determine the structure of pre–white dwarfs and white dwarfs over much of their cooling history. Finally, white dwarfs are structurally simple compared to other stars. If we can perform asteroseismology at all, these are the stars to start with.

Learning about the structure of white-dwarf stars can help to answer some of the most pressing questions in astrophysics. It will allow us to learn more about the $^{12}C(\alpha, \gamma)^{16}O$ reaction rate (Caughlan & Fowler 1988) and how mass is lost as a star evolves from the asymptotic giant branch (AGB) to the white dwarf cooling track (Iben 1989; D'Antona & Mazzitelli 1991), and we can test the predictions of spectral evolution theory (Fontaine & Wesemael 1987, 1991). Ultimately, knowledge of white-dwarf structure and cooling history will let us determine the history of star formation in the Galaxy (see Wood 1992) and the age of the Galactic disk and halo (Winget et al. 1987; Wood 1992).

Winget et al. (1991) made the first steps in the asteroseismology of compact objects with their analysis of the pulsating pre–white dwarf (DOV) PG 1159−035 using existing models and asymptotic theory. They determined the stellar mass, rotation rate, demonstrated that the outer layers are stratified, and set very low upper limits on the presence of a magnetic field.

Here we present the first asteroseismological determination of the structure of a DBV white dwarf, GD 358, from observations obtained with the Whole Earth Telescope (WET; Nather et al. 1990).

2. OBSERVATIONAL DATA FOR GD 358

GD 358 is the prototype of the first class of variable stars whose existence was predicted before their discovery. It is also the brightest known pulsating DB white dwarf. Since the discovery of its pulsations (Winget et al. 1982), it has been the object of considerable spectroscopic and photometric scrutiny. Analysis of optical and UV spectra (Koester, Weidemann, & Vauclair 1983; Koester et al. 1985; Liebert et al. 1986; Thejl, Vennes, & Shipman 1991) show that the surface temperature is somewhere between 28 and 24×10^3 K, with $24 \pm 1 \times 10^3$ K being the currently accepted value, which we adopt as the effective temperature range for our model fitting process. A very rough mass estimate for GD 358 is available from the surface gravity ($\log g = 8.0 \pm 0.3$); this only says the mass is somewhere between 0.45 and 0.75 $M_{\odot}$.

Previous high-speed photometric studies (Winget et al. 1982; Hill 1986, 1987) show that the power spectrum of GD 358 is quite complex and its period structure in the Fourier transform does not repeat from night to night. This suggests that either the period structure is not resolved in these single site observations or that the period structure is inherently unstable on a timescale of days.

Winget et al. (1993, 1994) selected GD 358 as the primary target of the 1990 May WET run, to attempt to resolve the complicated pulsational behavior and analyze the structure of a DBV star with asteroseismology. The results were spectacular. With over 150 hours of high-speed photometry over an 11

[1] Current Address: X-2, MS B-220, Los Alamos National Laboratory, Los Alamos, NM 87545.

TABLE 1

OBSERVED $\ell = 1$, $m = 0$ PULSATION PERIODS OF GD 358

k	P (s)	ΔP (s)	dP (s)	Amplitude (mma)
18.....	(810.7)	(44.1)	+3.78	4.78
17.....	770.7	40.0	+4.64	14.52
16.....	734.3	36.4	+1.81	3.46
15.....	770.6	33.6	−3.73	19.03
14.....	658.4	42.2	−0.64	8.35
13.....	618.3	40.1	+0.23	5.78
12.....	(576.8)	41.5	+2.55	1.28
11.....	(541.8)	35.0	−1.64	1.14
10.....	(501.6)	40.2	−0.68	1.09
9.....	464.2	37.4	−2.52	4.53
8.....	423.3	40.9	−0.76	4.98

NOTE.—Periods of less certain modes are in parentheses.

day span, they obtained a duty cycle of nearly 60% and resolved the light curve into 180+ modes. They interpret the largest amplitude peaks in the power spectrum—between 400 and 1000 s—as a series of consecutive overtone $\ell = 1$ g-modes based on the observed period spacings and similarities in the fine-structure splitting. We refer the reader to Winget et al. (1993) and references therein for details concerning photometric observations and analysis of the data on GD 358.

Our analysis confirms the $\ell = 1$ identity of the large amplitude peaks. The set of $\ell = 1$, $m = 0$ mode periods, period spacings, and amplitudes from Winget et al. (in units of millimodulation amplitudes (see Table 1 and Fig. 1) comprises the observational data for our asteroseismological analysis. We compare model and observational periods by two methods. First, we compare the deviations from uniform period spacing ($\equiv dP$) of the observations and models to determine the best-fitting model. We compute the deviations from uniform period spacing in the same way as Winget et al. (1994); we use the mean period spacing to define the nominal period of the $m = 0$ component of each observed mode. We use the mean period defined by the 39.2 s average of the period spacings derived from the Fourier transform of the period transform. We then compute the residuals from the mean period spacing and average them to determine the systematic offset. We obtain our final deviations from the mean period spacing (see Table 1) by subtracting this offset from each residual; the average of the deviations is now zero. We note that the deviations from the mean period spacing *must* be computed in the same manner for both observations and the model in order to make a meaningful comparison. Thus, in our models we consider only the modes corresponding to observed ones. In spite of the computational complexities, derivations from the mean period spacing have the advantage that an uncertain observed period causes only one uncertain dP value.

We also computed period spacing diagrams using forward differencing

$$\Delta P_k = P_{k+1} - P_k$$

as presented by Bradley, Winget, & Wood (1993, hereafter BWW). In this case, there are no computational ambiguities, and we can use the extra periods present in the model to predict what the missing observed period spacings may be. The disadvantage is that we require a consecutive set of observed modes, to determine the period spacings. We present plots of dP and ΔP versus P for clarity, but comment at the outset that the parameters of our best-fitting model *do not* depend on the method of presentation.

3. THEORETICAL TOOLS

The evolutionary white-dwarf models and asteroseismological tools we use in this analysis are covered in detail by BWW and references therein. We present only a brief outline of our models and methods here.

We use evolutionary white-dwarf models computed from an updated version of the White Dwarf Evolutionary Code (WDEC), described by Lamb & Van Horn (1975), Wood (1990), and BWW. With this code, we can construct models with carbon-oxygen cores of varying ratios and different helium layer masses. It includes energy losses due to neutrino emission. We include helium/carbon composition profiles using a parameterization of the diffusive equilibrium profiles of Arcouragi & Fontaine (1980) as described by BWW. We treat convection within the framework of mixing-length theory, using the ML2 version of convection (see TFW for a description) for all of our models, because the pulsation periods are not dependent on the convective efficiency.

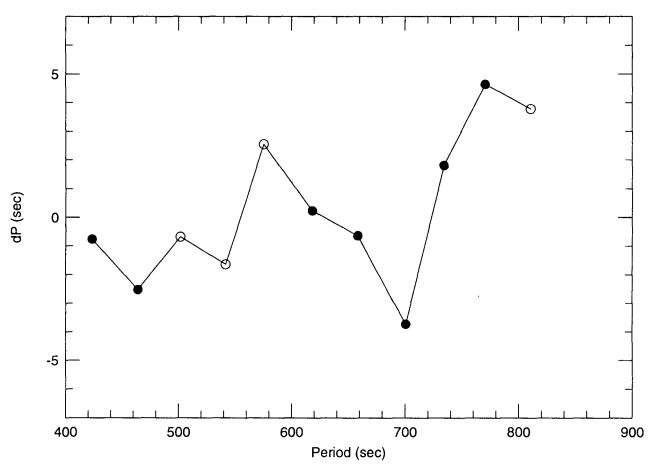

FIG. 1a

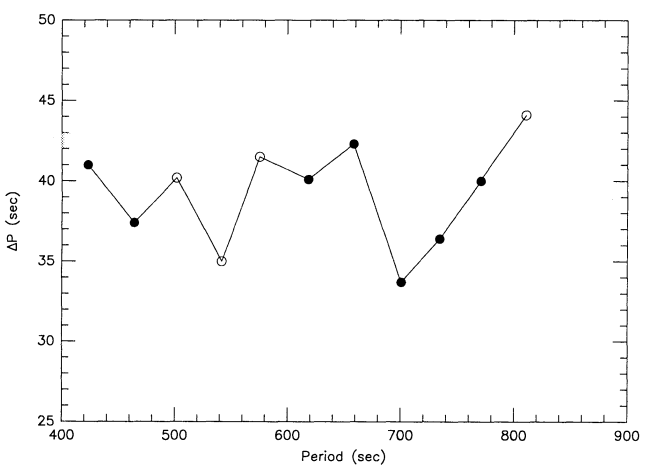

FIG. 1b

FIG. 1.—(*a*) Period spacing vs. deviations from uniform period spacing (dP diagram) for GD 358 observational data, using a mean period spacing of 39.2 s. dP values resulting from less certain periods are denoted by open dots. (*b*) Same as (*a*), but for period spacings (ΔP).

For our pulsation analysis, we solve the nonradial oscillation equations in the adiabatic approximation using a fourth-order Runge-Kutta-Fehlberg (RKF) integrator code with error limiters (Kawaler, Hansen, & Winget 1985). RKF also has the ability to interpolate extra zones into an equilibrium model until it is satisfied the nodes of an eigenfunction are resolved, so RKF continues to perform well on high-overtone modes. We solve for the pulsation periods (P), kinetic energies of oscillation (KE), the four eigenfunctions, and the nonradial weight functions described by Kawaler et al. (1985). For details concerning the derivation of the nonradial pulsation equations and the numerical methods used to solve them, see Unno et al. (1989) and Kawaler et al. (1985).

4. THE INTERNAL STRUCTURE AND OTHER PARAMETERS OF GD 358

We use a two-step procedure to determine the structure of GD 358. First, we determine a trial stellar mass from the mean period spacing and trial helium layer masses via trapped mode periods. This is the *forward method* for seismology, in contrast to inversion procedures commonly used by geologists and helioseismologists. Using the observed mean period spacing of 39.5 ± 5.2 s and the model sequences of BWW, we find $\sim 0.6\ M_\odot$ models have mean period spacings near 39 s at $T_{\rm eff} = 24{,}000$ K.

We constrain the thickness of the helium layer via the analytical relation for the periods of trapped modes developed by C. J. Hansen (1987, private communication) and elaborated on by Kawaler (1990), Kawaler & Weiss (1991), Brassard et al. (1992), and BWW. Observationally, trapped modes show up as minima in both plots of deviations from uniform period spacing (dP diagram) and period spacing diagrams (ΔP diagram), as shown in Figure 1. Trapped modes cause minima because the neighboring modes are pulled toward the resonance, resulting in periods close to that of the trapped mode. GD 358 has a pronounced minima at 700.6 s in both plots. If we use this period in the trapped mode period relation, we derive possible helium layer masses of 10^{-7}, 2×10^{-6}, and $10^{-5}\ M_*$. A comparison of the observations with the figures in BWW suggests that helium layer masses near $10^{-6}\ M_*$ best duplicate the observed dP and ΔP pattern.

4.1. *Structural Parameters of GD 358*

With constraints on the stellar mass and helium layer mass in hand, we begin our detailed matching, using the observed dP and ΔP diagrams of GD 358 as our target. While we cover a fairly extensive region of parameter space, we find that simply averaging the difference between the periods and period spacings of the models and observations suffices to determine which model provides the best fit. We define our best-fitting model as the one whose period and period spacing differences are the smallest *and* has the correct trapping cycle. We consider only the largest amplitude peaks that lie between 600 and 770 s and those at 423 s and 464 s in our formal statistical analysis. The other peaks are more uncertain because of their smaller amplitudes or because not all three members of the $\ell = 1$ triplet from each mode (due to slow rotation) are present.

We seek to match the large minimum in dP (and ΔP), with a trapping amplitude of 8.4 s, and relatively flat region below 600 s. Although we only have one pronounced dP (or ΔP) minimum, we can use the absence of other significant minima to place a lower limit on the trapping cycle. As BWW describe in detail, the trapping cycle is most sensitive to the helium layer mass, while the trapping amplitude tells us about the transition zone thickness. Finally, we can constrain the effective temperature (luminosity) by lining up the theoretical dP (ΔP) minimum with the observed one.

We first attempt to fit the observations with pure carbon core models to further constrain the helium layer mass and to test the need for a second interface. The best fits to the dP (and ΔP) minima centered at 700 s occur when $M_{\rm He} \sim 2 \times 10^{-6}\ M_*$. Models with $M_{\rm He} \sim 10^{-(4-5)}\ M_*$ have trapping cycles that are too short to accommodate the rising deviations between 700 and 800 s (see Fig. 2). When we also consider the dP (or ΔP) values between 400 and 500 s, models with $M_{\rm He} = 1.5\text{–}2 \times 10^{-6}\ M_*$ still fit the best. Our derived helium layer mass does not change if we consider the values for the uncertain periods or their alternatives between 500 and 600 s, but our models fail to duplicate the details in the observed dP or ΔP distribution. Models with pure carbon cores lack the extra "structure" in their dP and ΔP diagrams, and they have a minimum near 500 s instead of the observed 542 s. However, our statistical analysis uses *only* the certain dP or ΔP values and shows the carbon core models have some of the best overall fits due to the excellent fit of the region between 658 and 810 s. The less certain, small minima at 464 and 542 s and the slight dip at 618 s suggests that two interfaces are present, because our experience (see BWW) indicates that modes trapped by a single interface will have a smoothly varying run of dP or ΔP.

When we include C/O cores in our models, we find once again that models with $M_{\rm He} \sim 10^{-4}$ or $10^{-5}\ M_*$ have trapping cycles that are too short (~ 3 modes). The presence of a rapid change in the C/O abundance with mass produce the effect of a second interface, and resonances between the He/C and C/O interface can result. This can lead to beating between the trapping of cycles of the He/C and C/O interfaces. The beat cycle produces a series of shallow minima followed by a series of deep minima, with an overall trapping cycle of ~ 3 modes. Thus, we conclude the observed run of dP and ΔP values cannot be replicated with models having helium layer masses thicker than $10^{-5}\ M_*$.

We then examine models with helium layers near $2 \times 10^{-6}\ M_*$ and different C/O core abundances and profiles. These models match the central minimum at 700 s pretty well, and some also duplicate the secondary minimum around 464 s. All of the models have problems matching the less certain minimum at 542 s. We find two possible C/O profile models whose dP and ΔP values fit the observational data best (see Fig. 3). One model has a 50:50 C/O core extending to $0.8\ M_*$ with a steep C/O transition region and a helium layer mass of $2 \times 10^{-6}\ M_*$. The second model has a broader C/O transition region than the first model and a helium layer mass of $1.5 \times 10^{-6}\ M_*$. Statistically, the first model has a marginally better period match, and we use the parameters from this model in Table 2. There is a slight variation of acceptable helium layer masses when we vary the stellar mass; lower mass models require slightly thinner helium layers. Even so, the range of allowable helium layer masses is small: 1–3 $\times 10^{-6}\ M_*$.

While we use the less certain/lower amplitude peaks to infer the presence of a C/O interface, we emphasize that these periods do not affect our inferred helium layer mass, because we had an experience with model fitting using a different period for the mode near 542 s. Due to an earlier misidentifica-

1994ApJ...430..850B

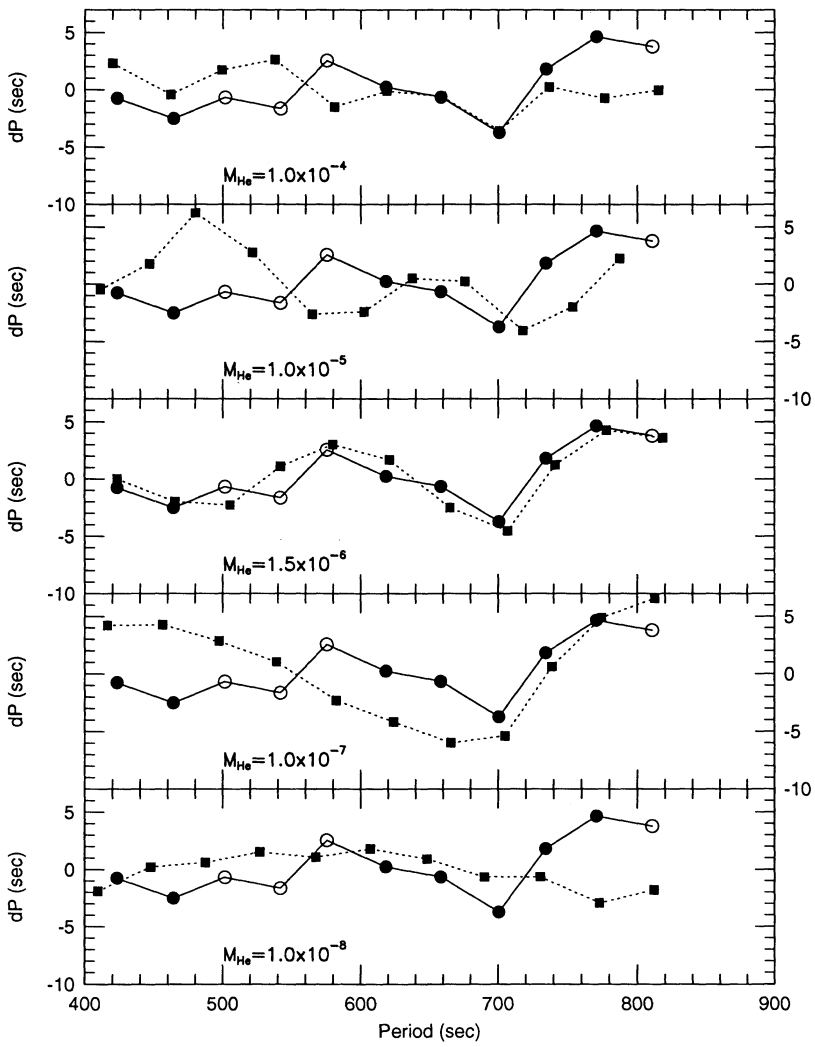

FIG. 2*a*

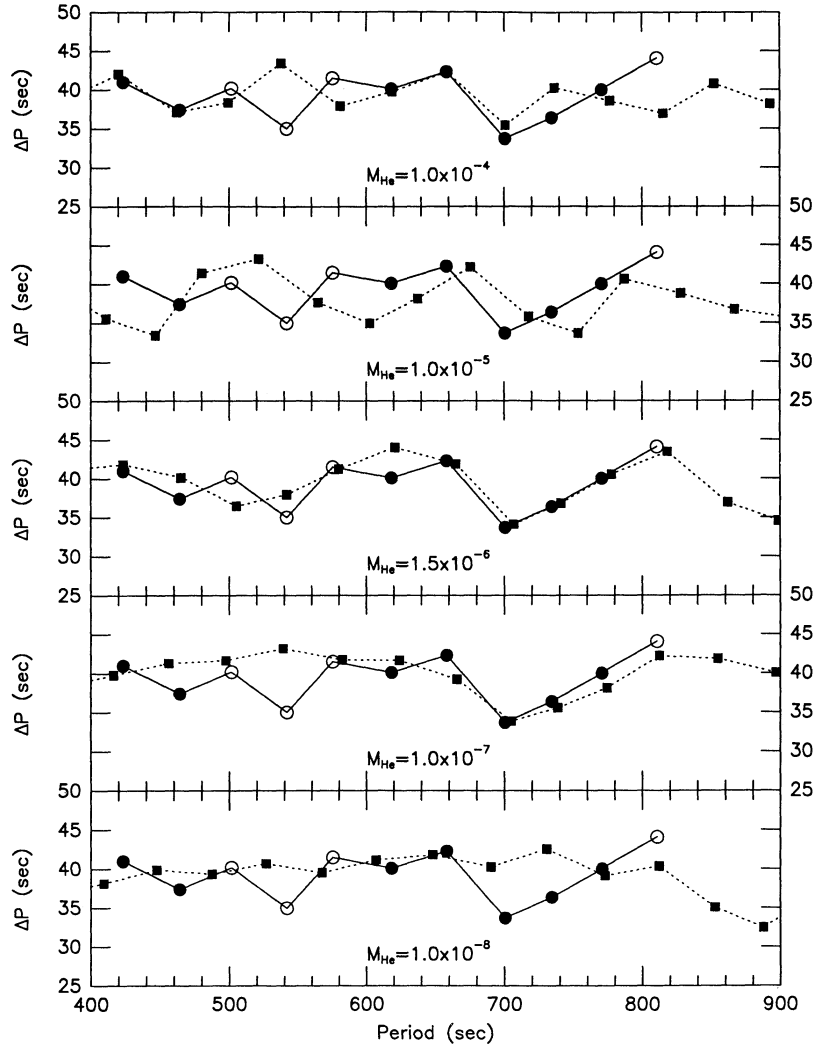

FIG. 2*b*

FIG. 2.—(*a*) Theorectical *dP* vs. *P* diagrams (*squares and dashed lines*) of 0.6 $M_{\odot}$ models with differing helium layer masses compared to the observational data for GD 358 (*dots*). The model with $M_{He} \sim 10^{-6}\ M_{*}$ best duplicates the observations. (*b*) Same as (*a*), but for period spacings (ΔP).

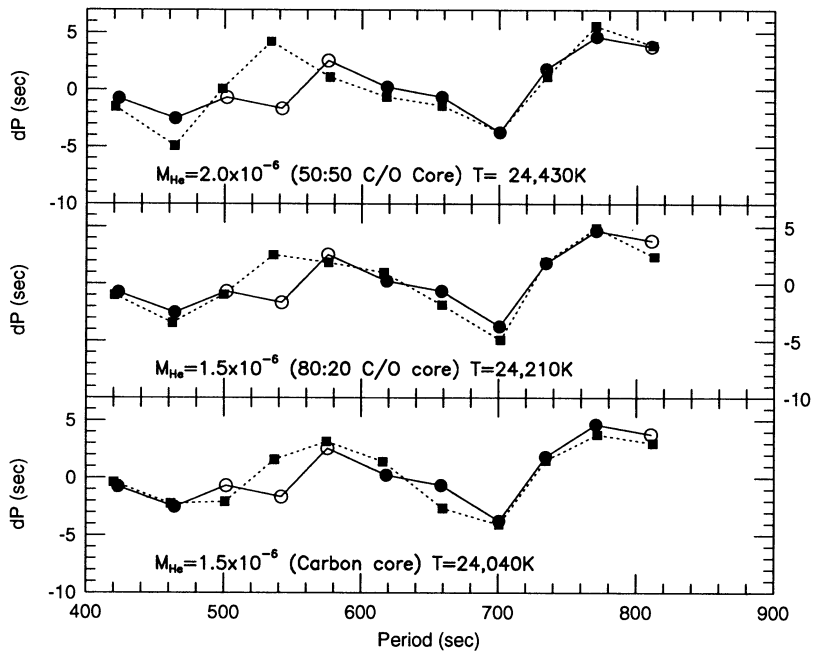

FIG. 3*a*

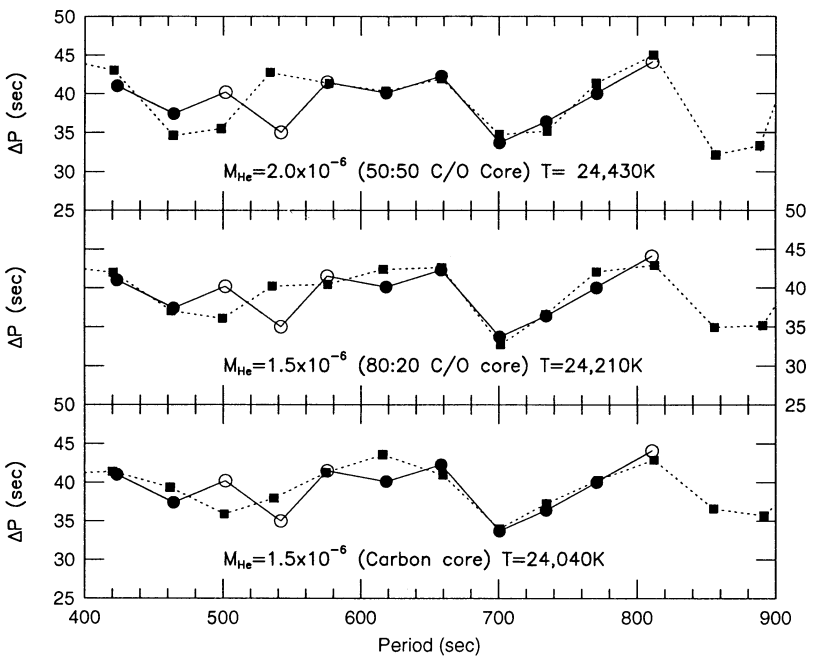

FIG. 3*b*

FIG. 3.—(*a*) *dP* diagrams for our "best-fit" models (*dashed lines and spares*) vs. the observations (*dots*). They have masses of 0.61 $M_{\odot}$, and helium layer masses as indicated in the panel. Both have 50:50 C/O cores extending to ~0.8 M_{*}, but the model in the middle panel has a slightly shallower profile. We show our best-fitting pure carbon core model in the bottom panel for comparison. (*b*) Same as (*a*), but for period spacings (ΔP).

tion, we used 546.0 s instead of 541.8 s as the observed period. This created a deep minimum in ΔP at 546 s. Even then, the best-fitting model wound up having a helium layer mass of 1.5–2 × 10^{-6} M_{*}, although we were unable to adjust the C/O core profile to get as good a fit as we do now. Thus, our bottom line is we get a unique helium layer mass, but proof of a C/O transition zone lies in the less certain period region between 500 and 600 s.

We then vary the thickness of the He/C transition zone in our models using our best-fit helium layer mass to obtain the best match between the observed and theoretical *dP* and ΔP diagrams. In all cases, models with relatively thin He/C transition zones (~8 pressure scale heights) fit the observed data best. While the extension of the carbon "tail" into the helium layer is consistent with the expectations of diffusive equilibrium (see Pelletier et al. 1986), the helium "tail" is much smaller than diffusive equilibrium profiles predict. This is not a surprise, since GD 358 is young enough that diffusive equi-

TABLE 2

BEST-FIT MODEL AND OBSERVATIONS FOR GD 358

Parameter	Evolutionary Model	GD 358
$\langle \Delta P \rangle$ (s)	39.6 ± 3.4	39.5 ± 5.2
$T_{\rm eff}$ ($\times 10^3$)	24 ± 1	24 ± 1
$\log g$	8.0 ± 0.1	8.0 ± 0.3
$M/M_\odot$	0.61 ± 0.03	0.60 ± 0.17
$R/R_\odot$	0.0127 ± 0.0004	0.0128 ± 0.0025
$\log (L/L_\odot)$	$-1.30^{+0.09}_{-0.12}$	$-1.32^{+0.17}_{-0.27}$
Bolometric correction	$-2.58^{+0.25}_{-0.13}$	n.a.
Distance (pc)	42 ± 3	36 ± 4
$\log M_{\rm He}/M_*$	$-5.70^{+0.18}_{-0.30}$	n.a.
Transition zone thickness	~ 8 PSH	n.a.

librium should not be established in the core yet. We confirm this with estimates of the diffusion timescale at the base of the helium tail; it is comparable to the evolutionary timescale of $\sim 3 \times 10^7$ yr. This suggests that we might have the possibility of determining the depth of the transition zone and directly test diffusion theory. We need to analyze the structure of other DBV white dwarfs to confirm this possibility.

Finally, we vary the stellar mass of our models to determine the range of stellar masses with good fits that lie within our acceptable temperature range. We did not try to obtain as rigorous a "best fit" here as we did for the 0.61 $M_\odot$ models. This procedure gives us an acceptable mass range of 0.58–0.63 $M_\odot$ (see Fig. 4) and a helium layer mass range of $1–3 \times 10^{-6}$ M_*, with the effective temperature of the best-fit model increasing as the stellar mass decreases. Our uncertainties in the stellar mass and other global quantities are dominated by the uncertainty in the effective temperature determination. Roughly speaking, halving the effective temperature uncertainty would halve the uncertainties in our derived model parameters.

We summarize the parameters of our best-fitting model for GD 358 along with structural values determined from other observations in Table 2.

4.2. *The Distance to GD 358*

Our model fitting procedure also provides us with the luminosity and radius of our best model (see Table 2). Using the luminosity and the appropriate bolometric correction factor of ~ -2.6 mag (computed from model atmosphere fluxes kindly provided by D. Koester), we can derive a distance to GD 358 (see Appendix) that is *independent of the trigonometric parallax.* Like the other quantities, the error in our distance determination is dominated by the uncertainty in the effective temperature. Our distance is 42 ± 3 pc, consistent with the 36 ± 4 pc derived from recent parallax values (Harrington et al. 1985). This shows that asteroseismology not only gives us information about the internal structure of stars, but also provides us with independently determined values for other fundamental quantities, like the distance.

The reliability of our seismological structure determination is only as good as our mode identification. For example, the modes could be consecutive overtones, but arise from a different ℓ value. If these are consecutive $\ell = 2$ modes, our derived stellar mass would be around 0.2 $M_\odot$, inconsistent with the spectroscopic log g value. It would also make GD 358 the lowest mass field white dwarf known. Because of the larger radius, the lower mass model would be much more luminous; we would derive a distance of ~ 75 pc, completely at odds with the parallax value. This provides us with a separate confirmation of the mode identification made earlier.

The mass discrepancy only gets worse if we consider the observed modes as being consecutive overtone modes with even higher ℓ values, and we also have to deal with increasingly severe geometric cancellation effects. If the observed modes are another ℓ and only every other overtone is excited, we would have a very long (>10) mode trapping cycle. This would require models with $M_{\rm He} < 10^{-8}$ M_*, below the minimum helium layer mass required for pulsational instability. Our principal problem is some modes have low amplitudes, so that some observed dP values could be in error. However, the central minimum is determined by large amplitude modes, and the presence of a relatively flat dP region between 400 and 600 s is reasonably secure. Our data clearly indicate the presence of a mode trapping source near 2×10^{-6} M_* in mass, which we interpret as the helium/carbon interface.

5. ASTROPHYSICAL CONSEQUENCES

Our newfound knowledge of the structure of a DB white dwarf finally gives us observational data to compare to theoretical predications of white dwarf evolution. We can also compare the derived structural parameters for GD 358 with other observational data.

All of our best-fitting models that fit the observed effective temperature, mean period spacing, and period distribution yield the same radial overtone (k value) mode assignment presented in Table 1. This, coupled with the agreement between the seismological and parallax distance, implies that our mode identification is secure and there is no ambiguity in the radial overtone number of the observed modes.

The mass of GD 358 is consistent with the mean mass of 0.55 ± 0.10 $M_\odot$ derived by Oke, Weidemann, & Kester (1984) for DB white dwarfs through multichannel photometry. It is also consistent with the mean mass of DA white dwarfs found by Bergeron, Saffer, & Liebert (1992). Our mass determination and effective temperatures give us radii and luminosities consistent with our expectations for white dwarfs.

The helium layer mass is *much* smaller than predicted by stellar evolution theory (Iben 1989; D'Antona & Mazzitelli 1991) and thinner than the helium layers derived by Pelletier et al. (1986). Unless the mode identification or model fitting is in error, we must consider how Nature can make a star like GD 358 and what it will eventually become. While 10^{-2} M_* is the "canonical" helium layer mass suggested by stellar evolution theory, *any* helium layer mass thinner than this can be made consistent, depending on the relationship between the initiation of the "superwind" and the helium shell flash cycle (Kawaler 1987). Our helium layer mass is telling us that mass loss does not cease when the helium layer mass becomes too thin for helium shell flashes to occur. This may imply that the mass-loss process is dynamical rather than quasi-static.

More troubling is our disagreement with the results of Pelletier et al. According to their calculations and confirmed by our models, the base of the convection zone should very nearly reach the middle of a He/C transition zone located at $\sim 2 \times 10^{-6}$ M_*. If all the carbon stirred up by the convection zone is uniformly mixed throughout the convection zone, then GD 358 should become a white dwarf with a spectrum with significant carbon features, because $N(\rm C)/N(\rm He) \sim 0.05–0.25$, greater than the observed ratios of 10^{-2} to 10^{-6}. In the temperature range of the DQ stars (12–6,000 K), convection is nearly adiabatic, so we cannot appeal to our ignorance of

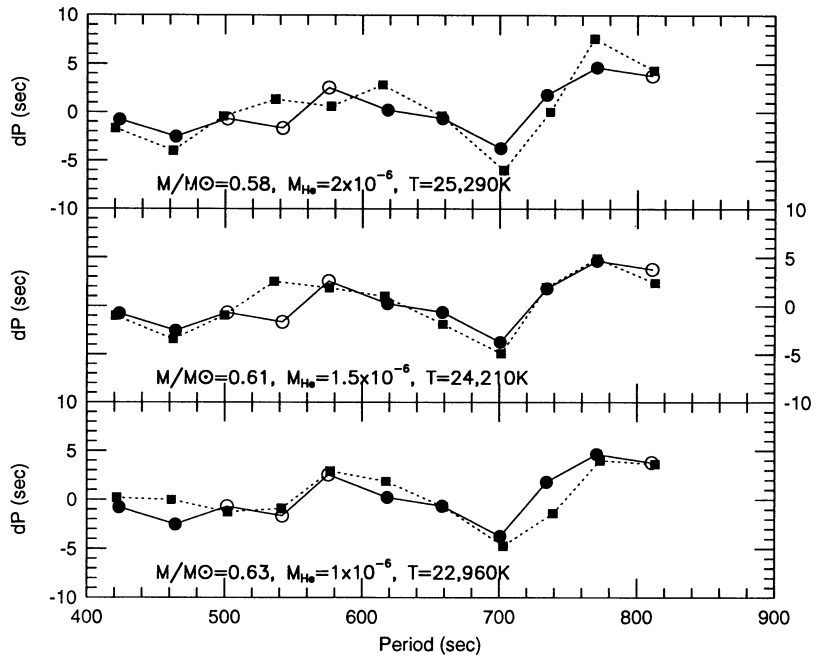

FIG. 4*a*

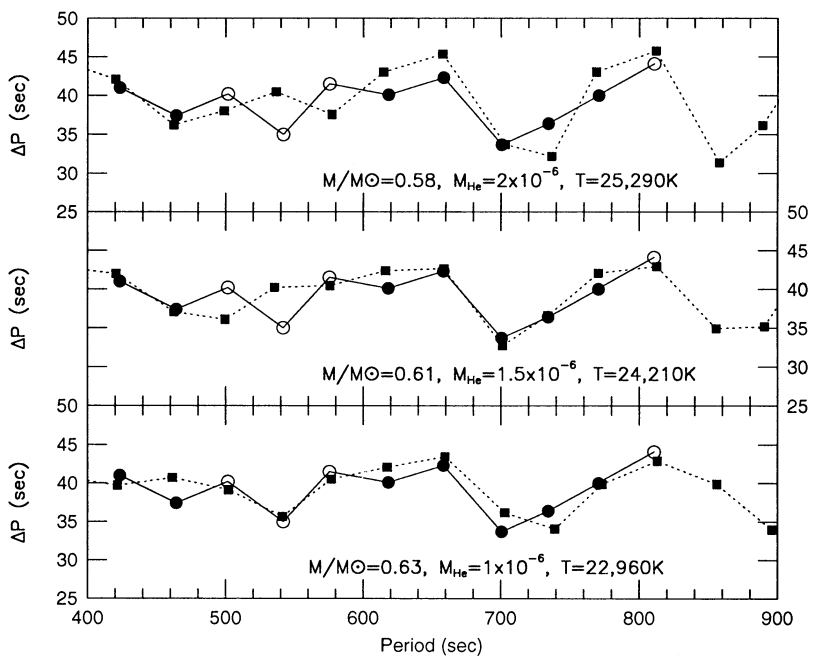

FIG. 4*b*

FIG. 4.—(*a*) Theoretical *dP* vs. *P* diagrams (*squares and dashed lines*) of different stellar mass models compared to the observational data for GD 358. Below 0.58 $M_\odot$ and above 0.63 $M_\odot$ the "best fitting" models lie outside of our acceptable temperature range. (*b*) Same as (*a*), but for period spacings (ΔP).

convection theory here. However, diffusion is still trying to bring the carbon back down, and it is not clear exactly how this will affect the dredging up of carbon in the helium convection zone. We are left with three choices: either the carbon stirred up by the convection zone is *not* dredged up to the surface efficiently and the mean helium layer mass derived by Pelletier et al. is too large; or GD 358 is unique, and not an ancestor of any known class of cool white dwarf. Finally, it might be possible that some other mode trapping agent is located at $2 \times 10^{-6}\ M_*$ in our model—such as a magnetic field—and the helium layer mass is actually about $10^{-4}\ M_*$. Seismologically determined helium layer masses from other DBV stars are imperative to help us settle this question. Promising candidates include PG 1115+158, PG 1456+103, and PG 1654+160.

Alternatively, it may be that the convection zone itself generates a magnetic field (as modeled by Markiel, Thomas, & Van Horn 1994), in which case the convection penetrates only deep enough to generate a field of order 10^5 G, and then it will stop. This could seriously alter the results of Pelletier et al., and also

have an effect on white dwarf ages as derived from cooling calculations.

We are grateful to C. J. Hansen, S. D. Kawaler, R. E. Nather, and M. A. Wood for their encouragement and many discussions. We also thank D. Koester for supplying us with DB model atmosphere results for accurate bolometric corrections. P. A. B. thanks the University of Texas for a graduate student fellowship during the past 2 years that allowed him to work with a minimum of distractions. Finally, we wish to thank the other members of the Whole Earth Telescope collaboration for collecting and analyzing the data that made this work possible. This research was supported by the National Science Foundation under grants 86-00507 and 90-14655 through the University of Texas and McDonald Observatory.

APPENDIX

For clarity, we describe our procedure for determining the distance to GD 358 using our seismologically determined luminosity values. Using model atmosphere data kindly supplied by D. Koester and assuming $M_{\odot\mathrm{Bol}} = 4.75$ (Allen 1973) we obtain bolometric corrections of -2.71 mag at 25,000 K, -2.58 mag at 24,000 K, and -2.33 mag at 23,000 K. We then use

$$M_{\mathrm{bol}} = M_{\odot\mathrm{Bol}} - 2.5 \log (L/L_{\odot})$$

to determine the absolute bolometric magnitude of GD 358 using the luminosity data of Table 2. Inserting numbers and using $M_{\odot\mathrm{Bol}} = 4.75$, we obtain bolometric absolute magnitudes ranging from $M_{\mathrm{Bol}} = 7.69$ to 8.35 with a "best" value of 7.97. Now we use the distance modulus formula

$$m_V - M_V = 5 \log d(\mathrm{pc}) - 5$$

to derive the distance to GD 358 in parsecs, using $m_V = 13.65$ (Winget et al. 1982). Our "best" distance is 42 pc, with a range from 45 to 39 pc.

Our distance uncertainty is only $\sim 7\%$, whereas the luminosity uncertainty is $\sim 24\%$. Two factors cause the change in the size of the uncertainty. First, the distance varies as the square root of the luminosity, which means the distance uncertainty should be roughly half the uncertainty in luminosity. Also, the change in bolometric correction with effective temperature acts to partly cancel out some of the luminosity uncertainty in the distance. If we had used a constant bolometric correction of -2.48 mags, the distance would have been 42 ± 5 pc ($\sim 12\%$ uncertainty) instead of the 42 ± 3 pc ($\sim 7\%$ uncertainty) we derive.

REFERENCES

Allen, C. W., ed. 1973, Astrophysical Quantities (3d ed.; London: Athlone)
Arcouragi, J.-P., & Fontaine, G. 1980, ApJ, 242, 1208
Bergeron, P., Saffer, R. A., & Liebert, J. 1992, ApJ, 394, 228
Bradley, P. A., Winget, D. E., & Wood, M. A. 1993, ApJ, 406, 661 (BWW)
Brassard, P., Fontaine, G., Wesemael, F., & Hansen, C. J. 1992, ApJS, 80, 369
Caughlan, G. R., & Fowler, W. A. 1988, Atomic Nucl. Data Tables, 40, 334
D'Antona, F., & Mazzitelli, I. 1991, in IAU Symp. 145, Evolution of Stars: The Photospheric Abundance Connection, ed. G. Michaud & A. Tutukov (Dordrecht: Kluwer), 399
Fontaine, G., & Wesemael, F. 1987, in IAU Colloq. 95, 2d Conf. on Faint Blue Stars, ed. A. G. D. Philip, D. S. Hayes, & J. Liebert (Schenectady: Davis), 319
———. 1991, in IAU Symp. 145, Evolution of Stars: The Photospheric Abundance Connection, ed. G. Michaud & A. Tutukov (Dordrecht: Reidel), 421
Harrington, R. S., et al. 1985, AJ, 90, 123
Hill, J. A. 1986, M.A. thesis, Univ. Texas
———. 1987, in IAU Colloq. 95, 2d Conf. on Faint Blue Stars, ed. A. G. D. Philip, D. S. Hayes, & J. Liebert (Schenectady: Davis), 681
Iben, I., Jr. 1989, in IAU Colloq. 106, Evolution of Peculiar Red Giant Stars, ed. H. R. Johnson & B. Zuckerman (Cambridge: Cambridge Univ. Press), 205
Kawaler, S. D. 1987, in IAU Colloq. 95, 2d Conf. on Faint Blue Stars, ed. A. G. D. Philip, D. S. Hayes, & J. Liebert (Schenectady: Davis), 297
———. 1990, in Confrontation Between Stellar Pulsation and Evolution, ed. C. Cacciari & G. Clementini (ASP Conf. Ser. 11), 494
Kawaler, S. D., Hansen, C. J., & Winget, D. E. 1985, ApJ, 295, 547
Kawaler, S. D., & Weiss, P. 1990, in Proc. Oji International Seminar, Progress of Seismology of the Sun and Stars, ed. Y. Osaki & H. Shibahashi (Berlin: Springer), 431
Koester, D., Vauclair, G., Dolez, N., Oke, J. B., Greenstein, J. L., & Weidemann, V. 1985, A&A, 149, 423
Koester, D., Weidemann, V., & Vauclair, G. 1983, A&A, 123, L11
Lamb, D. Q., & Van Horn, H. M. 1975, ApJ, 200, 306
Liebert, J., Wesemael, F., Hansen, C. J., Fontaine, G., Shipman, H. L., Sion, E. M., Winget, D. E., & Green, R. F. 1986, ApJ, 309, 241
Markiel, J. A., Thomas, J. H., & Van Horn, H. M. 1994, ApJ, 430, 834
Nather, R. E. Winget, D. E., Clemens, J. C., Hansen, C. J., & Hine, B. P. 1990, ApJ, 361, 309
Oke, J. B., Weidemann, V., & Koester, D. 1984, ApJ, 281, 276
Pelletier, G., Fontaine, G., Wesemael, F., Michaud, G., & Wegner, G. 1986, ApJ, 307, 242
Thejl, P., Vennes, S., & Shipman, H. L. 1991, ApJ, 370, 355
Unno, W., Osaki, Y., Ando, H., Saio, H., & Shibahashi, H. 1989, Nonradial Oscillations of Stars (2d. ed.; Tokyo: Univ. Tokyo Press)
Winget, D. E., Hansen, C. J., Liebert, J., Van Horn, H. M., Fontaine, G., Nather, R. E., Kepler, S. O., & Lamb, D. Q. 1987, ApJ, 315, L77
Winget, D. E., et al. 1991, ApJ, 378, 326
———. 1993, in IAU Colloq. 137, Inside the Stars, ed. W. W. Wiess & A. Baglin (ASP Conf. Ser. 40), 789
———. 1994, ApJ, 430, 839
Winget, D. E., Robinson, E. L., Nather, R. E., & Fontaine, G. 1982, ApJ, 262, L11
Winget, D. E., Van Horn, H. M., Tassoul, M., & Fontaine, G. 1983, ApJ, 268, L33
Wood, M. A. 1990, Ph.D. thesis, Univ. Texas
———. 1992, ApJ, 386, 539